J Membrane Biol (2008) 222:43–54
DOI 10.1007/s00232-008-9098-4

LETTER TO THE EDITOR

A Variant of the Ca^{2+}-Activated Cl Channel Best3 is Expressed in Mouse Exocrine Glands

Alaka Srivastava · Victor G. Romanenko · Mireya Gonzalez-Begne · Marcelo A. Catalán · James E. Melvin

Received: 1 September 2007 / Accepted: 21 February 2008 / Published online: 15 April 2008

Abstract Fluid secretion by exocrine glands requires the activation of an apical Ca^{2+}-dependent Cl channel, the molecular identity of which is unknown. We found that mouse exocrine glands expressed an alternately spliced variant of *Best3*, a member of the *Bestrophin* (*Vmd2*) Ca^{2+}-activated Cl channel gene family, whereas the heart expressed full-length Best3. The spliced transcript lacked exons 2, 3 and 6 (Best3-Δ2,3,6) and is predicted to generate an in-frame protein missing the entire cytoplasmic N terminus, the initial two transmembrane domains and part of the first intracellular loop. In addition to exocrine glands, the Best3-Δ2,3,6 splice variant transcript was detected in lung, testis and kidney. The parotid gland and heart expressed proteins of the predicted size for Best3-Δ2,3,6 and full-length Best3, respectively, that targeted to the plasma membrane in HEK293 cells. HEK293 cells expressing Best3 displayed Ca^{2+}-dependent Cl^- currents that were sensitive to the Cl channel blocker DIDS. In contrast, no Ca^{2+}-dependent Cl^- currents were detected in cells expressing Best3-Δ2,3,6. Cotransfection of Best3-Δ2,3,6 with Best3 or Best2 (also expressed in salivary gland acinar cells) had no significant effects on the currents generated by either of these Ca^{2+}-dependent Cl channels. Our results demonstrate that exocrine glands express a unique splice variant of Best3. Nevertheless, Best3-Δ2,3,6 does not produce Ca^{2+}-dependent Cl^- currents, nor does it regulate the activity of Best2 or the full-length Best3 channel.

Keywords Anion channel · Bestrophin · Calcium-activated chloride channel · Localization · Patch clamp · Salivary gland

Introduction

According to the current fluid secretion model, transepithelial movement of Cl^- is the primary driving force for water and electrolyte movement by exocrine gland acinar cells (Melvin et al. 2005; Mircheff 1989). The electrophysiological fingerprints for at least four types of Cl channels have been identified in the plasma membrane of acinar cells, including channels that are activated by either Ca^{2+}, cAMP, hyperpolarization or cell swelling (Arreola et al. 1996a, b; Kidd and Thorn 2000; Kotera and Brown 1993; Sundermeier et al. 2002; Zeng et al. 1997). A Ca^{2+}-gated Cl channel appears to be the major apical Cl^- efflux pathway in salivary gland acinar cells; however, the molecular identity of this channel has not been determined. Members of at least three distinct gene families (*CLCA*, *TTY* and *VMD2*) encode Ca^{2+}-activated Cl channels which could underlie the endogenous Ca^{2+}-dependent Cl^- currents in various tissues (Qu et al. 2003; Sun et al. 2002; Suzuki 2006; Tsunenari et al. 2003). Several CLCA channels are expressed in human and mouse salivary glands (Loewen and Forsyth 2005; Nakamoto et al. 2007). Unlike native Ca^{2+}-activated Cl channels, CLCA channels in heterologous expression systems generally require very high intracellular Ca^{2+} for activation (Eggermont 2004; Fuller and Benos 2000; Hartzell et al. 2005). Using an siRNA approach, suppression of CLCA expression in rat

Alaka Srivastava, Victor G. Romanenko, and Mireya Gonzalez-Begne have contributed equally to this work.

A. Srivastava · V. G. Romanenko · M. Gonzalez-Begne · M. A. Catalán · J. E. Melvin (✉)
Center for Oral Biology, Medical Center,
University of Rochester School of Medicine and Dentistry,
601 Elmwood Ave., Box 611, Rochester, NY 14642, USA
e-mail: james_melvin@urmc.rochester.edu

submandibular glands did not affect fluid secretion but did produce moderately elevated Cl^- levels in saliva, suggesting that CLCA may regulate Cl^- absorption by the duct cells in these organs (Ishibashi et al. 2006). Members of the *tweety* (*tty*) gene family in *Drosophila melanogaster* encode functional Ca^{2+}-activated Cl channels (Suzuki 2006), but the functional properties of mammalian homologues have not been evaluated.

Members of the *VMD2* gene family (vitelliform macular dystrophy type 2, also known as *BEST* or *Bestrophin*) are expressed in numerous murine and human epithelial cells in a pattern that is consistent with the expression of Ca^{2+}-activated Cl^- currents in these tissues (Barro Soria et al. 2006; Kunzelmann et al. 2007). Bestrophin channels share multiple functional and pharmacological properties with the Ca^{2+}-activated Cl channels in secretory acinar cells including low single-channel conductance (Chien et al. 2006; Martin 1993; Marty et al. 1984), activation at physiologically relevant Ca^{2+} concentrations (Arreola et al. 1996a, b; Evans and Marty 1986; Qu et al. 2004; Tsunenari et al. 2006), the same anion selectivity sequence (Ishikawa 1996; Perez-Cornejo et al. 2004; Qu et al. 2003) and sensitivity to a similar array of inhibitors (Arreola et al. 1998; Barro Soria et al. 2006; Ishikawa 1996; Qu et al. 2004). Moreover, interfering RNA for Best1 suppressed endogenous Ca^{2+}-activated Cl^- currents in airway and colonic epithelial cells, implying that *Best1* encodes a Ca^{2+}-activated Cl channel in these tissues (Barro Soria et al. 2006; Duta et al. 2004).

The human *Bestrophin* gene family consists of four members *BEST1–4* (also known as *VMD2*, *VMD2L1*, *VMD2L2* and *VMD2L3*) (Stohr et al. 2002; Sun et al. 2002; Tsunenari et al. 2003). Bestrophins are characterized by a highly conserved stretch of amino acid residues in the N-termini which contains four to six predicted transmembrane domains (Milenkovic et al. 2007; Qu et al. 2007; Sun et al. 2002; Tsunenari et al. 2003). In vitro expression of all four human Bestrophins generates Ca^{2+}-activated Cl^- currents (Tsunenari et al. 2003). Four *Bestrophin* homologues (*Best1–4*) are also present in the mouse genome (Kramer et al. 2004), although *Best3* appears to be a pseudogene based on the predicted translation product. Consequently, according to the HUGO and MGI nomenclature, the *Best3* pseudogene is no longer considered a functional member of the *Best* gene family; thus, it has been suggested that *Best4* (*Vmd2l3*) be henceforth termed *Best3* (see Qu et al. 2006; Qu et al. 2007). We therefore use the corrected nomenclature. Mouse *Best3*, which was first cloned from mouse heart (Kramer et al. 2004), contains 10 exons that encode for a 669–amino acid protein. Exon 1 encodes for much of the 5′-untranslated region, exons 2–9 include the sequence for the transmembrane domains, whereas exon 10 encodes most of the C-terminal domain of Best3 and the 3′-untranslated region. The first 369 N-terminal amino acids of Best3 are highly homologous to mouse Best1 and Best2. The N-terminal region of Best3 is 63% and 67% identical to Best1 and Best2, respectively (78% and 80% similar), but *Best3* has a unique C-terminus which lacks homology with Best1 and Best2 (Qu et al. 2006). Several splice variants of *Best3* have been observed in a number of tissues, e.g., brain, retina and kidney, whereas the full-length transcript appears to be exclusively expressed in the heart (Kramer et al. 2004). We found that exocrine glands express a splice variant of the Best3 Ca^{2+}-dependent Cl channel (Best3-Δ2,3,6) that lacks 132 amino acids in the critical N-terminal domain. Although Best3-Δ2,3,6 targets to the plasma membrane, its expression does not produce Ca^{2+}-dependent Cl^- currents, nor does it appear to regulate the functional properties of full-length Best2 or Best3.

Materials and Methods

HEK293 cells were obtained from ATCC (Manassas, VA). Tissues were dissected from BlackSwiss-129SvJ hybrid mice of either sex, aged 2–6 months, following protocols approved by the Animal Resources Committee of the University of Rochester and immediately frozen in liquid N_2. EZ-Link-Sulfo-NHS-SS biotin, immobilized neutravidin protein and dithiothreitol (DTT) were from Pierce (Rockford, IL). Glycine was from J. T. Baker (Philipsburg, NJ). All other reagents were from Sigma-Aldrich (St. Louis, MO) unless otherwise indicated.

RNA Isolation and Synthesis of cDNA

Total RNA was extracted from HEK293 cells or from 20 mg of tissue using RNeasy (Qiagen, Valencia, CA) according to the manufacturer's instructions. A modified RNA isolation protocol, which included proteinase K treatment for fibrous tissues, was used for the heart. First-strand cDNA was synthesized from 1 μg of total RNA in a 20-μl reaction using the iScript™ cDNA synthesis kit (Bio-Rad, Hercules, CA).

Polymerase chain reaction (PCR) amplification of 1.0 μl of cDNA was performed in a final volume of 25 μl using Taq-DNA polymerase reaction mix containing 2.5 μl of buffer (10x), 0.75 μl $MgCl_2$ (50 mM), 0.5 μl dNTP mix (10 mM), 0.1 μl *Taq* DNA polymerase and 1 μl (50 ng/μl) of forward and reverse primer sets. PCR products were purified using a PCR cleaning kit (Qiagen). Primers were designed based on the mouse *Best3* sequence (NCBI database, accession NM_001007583) and are listed in Table 1, while their location on the gene is shown in Fig. 1. Forward (F) and reverse (R) primers were also designed to

Table 1 Primer sets used to amplify different constructs of Best3 and Best3-Δ2,3,6

Primer set	Vector	Clone	Forward	Reverse
A	Exon 1–7		5′-TCACCAGTGAGGGTGGAAGC-3′	5′-GCGTACAGATCCAAGTCATGTC-3′
	Variant amplification		412–431	1332–1312
B	Exon 1–10		5′-TCACCAGTGAGGGTGGAAGC-3′	5′-CCGATTCCGGGACTGGTGCAG-3′
	Full-length amplification		412–431	2574–2554
C	pIRES2–EGFP	Best3	5′-GCTAGAATTCACAAAACCACCCACGATG-3′	5′-GAAGTCGACAAGTAGGGAGCTGGGTTAG-3′
			501–518	2540–2522
D	pIRES2–EGFP	Best3- Δ2,3,6	5′-GCGCGAATTCTCTTCCCTTGAGAGACT-3′	5′-GAAGTCGACAAGTAGGGAGCTGGGTTAG-3′
			468–487	2540–2522
E	pEGFPN1 pCI-neo	Best3	5′-CGCTGTGAATTCATGACTGTCACTTACTCCAG-3′	5′-CATAGTCGACTTGAACCAGGTCCTGGG-3′
			516–535	2522–2508
F	pEGFPN1 pCI-neo	Best3- Δ2,3,6	5′-CCTGAATTCATGCTCCTCATTTCCAGCAG-3′	5′-CATAGTCGACTTGAACCAGGTCCTGGG-3′
			834–853	2522–2508
G	Best3–EGFP fusion		5′-CGCTGTGAATTCATGACTGTCACTTACTCCAG-3′	5′-CTTTACTTGTACAGCTCGTCCATGCC-3′
			516–535	1400–1375, pEGFPN1 vector
H	Best3-Δ2,3,6–EGFP		5′-CCTGAATTCATGCTCCTCATTTCCAGCAG-3′	5′-CTTTACTTGTACAGCTCGTCCATGCC-3′
	Fusion		834–853	1400–1375, pEGFPN1 vector

Numbers reflect the location of primers on the Best3 mouse clone (accession NM_001007583) and the pEGFPN1 vector (accession U55762)

amplify mouse *Best1* (*Vmd2*, accession NM_011913), *Best2* (*Vmd2l1*, accession NM_145388), *BestPs* pseudogene (*Vmd2l2*, accession AY 450429) and *Best3* (*Vmd2l3*, accession NM_001007583) in acinar cells isolated from the mouse parotid gland: *Best1* F 5′-TTA AGG GTC TGG ACT TCT TG-3′, R 5′-CCT TAG TTT GGG AAA GAT CG-3′; *Best2* F 5′-CGCTGTTAAGGCGTAAAAACA-3′, R 5′-CCTCACAATTTCATGAGGTAGG-3′; *BestPs* F 5′-GAGGCAAAAGGGTCTCTGTG-3′, R 5′-GTTGAAAGT GGAATCCAGGAAG-3′; *Best3* F 5′-TTC TCA GCA GAC AGC CAT CAG-3′, R 5′-TTCCATGAAAGCCCCTGT GTG-3′.

The Best3 splice variants from different organs were amplified by PCR using primer set A (Table 1, Fig. 1a). Full-length cDNA from heart (Best3) and the alternate splice variant from the parotid gland (Best3-Δ2,3,6) were amplified using primer set B and cloned into the TOPO cloning vector (Invitrogen, Carlsbad, CA). Full-length Best3 and Best3-Δ2,3,6 were amplified using primer sets C and D, respectively, to incorporate *Eco*RI and *Sal*I restriction sites for subcloning into the pIRES2-EGFP (enhanced green fluorescent protein) expression vector (Clontech, Mountain View, CA). The bicistronic pIRES2-EGFP vector allows for identification of transfected cells by EGFP fluorescence. To generate Best-EGFP fusion proteins for localization studies, full-length Best3 and Best3-Δ2,3,6 were amplified using primer sets E and F, respectively, and cloned into the pEGFPN1 vector (Clontech). These latter primer sets incorporate *Eco*RI and *Sal*I restriction sites to permit in-frame expression of the insert with EGFP. The full-length Best3 amplified by primer set E was also inserted into the pCI neo mammalian expression vector to generate a stable cell line. The full-length EGFP-fused Best3 and Best3-Δ2,3,6 constructs in the pEGFPN1 vector were amplified using primer sets G and H, respectively (Table 1). All constructs were sequence-verified (Davis Sequencing, Davis, CA).

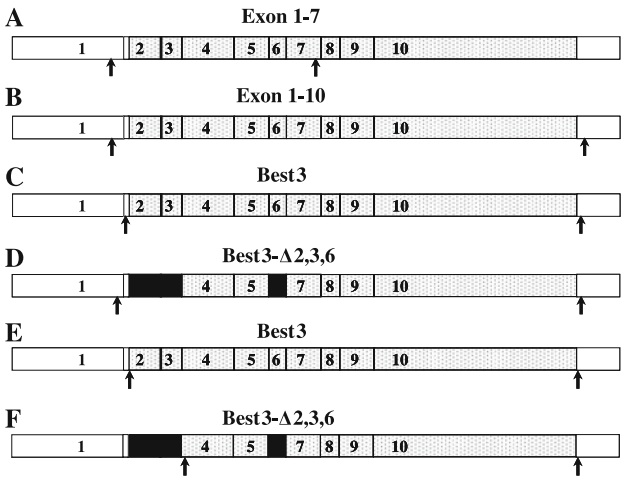

Fig. 1 Structure of mouse Best3 and Best3-Δ2,3,6 transcripts. The locations of primers used to amplify different constructs of Best3 are shown by *arrows*. Rows (**A–F**) correspond to primer sets A–F shown in Table 1. The full-length mRNA includes 10 exons (numbers 1–10). The translated region (cDNA) of each transcript is *shaded*. The missing exons in Best3-Δ2,3,6 are shown as *filled areas*

Cell Culture and Transient Transfection Conditions

HEK293 cells were maintained in growth medium (Dulbecco's modified Eagle medium supplemented with 10% fetal bovine serum) containing nonessential amino acids (0.1 mM), sodium pyruvate (1mM), L-glutamine (2 mM), penicillin and streptomycin (100 μg/ml of each antibiotic) at 37°C in a 5% CO_2 atmosphere humidified incubator. All ingredients were obtained from GIBCO/Invitrogen (Carlsbad, CA). For transient transfections, HEK293 cells were grown in either six-well plates (50–60% confluence) or T75 cm^2 flasks (80–85% confluent) and transfected (1 μg vector constructs/well or 5 μg of vector/flask) with lipofectamine (Invitrogen) in Opti-MEM® medium without serum according to the manufacturer's instructions. For stable expression of Best3, HEK293 cells were transfected with the full-length Best3-pCI neo vector. After 24 h of transfection, the cells were replated (1:10 dilution) and maintained in growth medium containing 1 mg/ml of Geneticin® (Invitrogen). After 4 days, individual colonies were transferred to 24-well plates, and after the fourth passage, the cell lines were considered stable. Best2-expressing HEK293 cells were kindly provided by Dr. Criss Hartzell (Emory University, Atlanta, GA).

EGFP and Immunofluorescence

HEK293 cells were grown to about 70% confluence in six-well plates containing poly-L-lysine-coated 1.0 cm-diameter glass coverslips and transfected with 1 μg of full-length Best-EGFP, Best-Δ2,3,6-EGFP or pEGFPN1 vector. Twenty-four hours after transfection, cells were washed with phosphate-buffered saline (PBS) and then stained for EGFP expression using a polyclonal, GFP-specific antibody (Molecular Probes/Invitrogen, Carlsbad, CA). To examine cell surface expression, intact cells were sequentially incubated at room temperature with 1.5% goat serum (in PBS, 30 min), anti-GFP antibody (1:200 for 45 min) and finally rhodamine-conjugated goat anti-rabbit IgG (1:20 for 30 min, Molecular Probes/Invitrogen). Primary and secondary antibodies were diluted in antibody diluent (Dako, Carpinteria, CA). For intracellular localization, the cells were fixed with 4% formaldehyde (30 min), permeabilized with 0.1% Triton X-100 in PBS and then labeled sequentially as above. The coverslips were mounted using Immu-mount (Thermo Electron, Waltham, CA). The fluorescence from cells expressing either the Best-EGFP, Best-Δ2,3,6–EGFP or

EGFP gene product was viewed with a Leica (Deerfield, IL) TCS SP Spectral Confocal upright microscope (model DMRE, x100 objective). EGFP was excited with the 488 nm wavelength (argon laser), and emitted fluorescence was monitored at >500 nm, whereas rhodamine was excited with 543 nm wavelength (HeNi laser), and emission was monitored at >580 nm. The estimated thickness of the images was 7 μm. Final images were processed with PhotoShop, version 7.01 (Adobe Systems, San Jose, CA).

Electrophysiology

Electrophysiological data were acquired using an Axopatch 200B amplifier and Digidata 1320A digitizer (Axon Instruments, Foster City, CA). Pipettes from Corning 8161 patch glass (Warner Instruments, Hamden, CT) were pulled to give a resistance of 2–3 MΩ in the solutions described below. The whole cell patch-clamp technique was used to record Cl^- currents from single HEK293 cells. As previously described (Qu et al. 2004), the bath solution contained (in mM) 140 NaCl, 5 KCl, 2 $CaCl_2$, 1 $MgCl_2$, 15 glucose and 10 HEPES, pH 7.3 with NaOH. In some experiments, 140 NaCl was substituted with 140 Na-glutamate in the bath solution. The pipette solution contained (mM) 146 CsCl, 2 $MgCl_2$, 5 EGTA, 4.5 $CaCl_2$, 8 HEPES and 10 sucrose, pH 7.3 (NMDG). The level of free Ca^{2+} was estimated to be 1 μM (WEBMAXC: http://www.stanford.edu/~cpatton/webmaxcShtm). Ca^{2+} was omitted in the "zero" Ca^{2+} pipette solution. In some experiments, the traditional Ca^{2+}-dependent Cl channel inhibitor 0.5 mM 4,4′-diisothiocyanatostilbene-2, 2′-disulfonic acid (DIDS) was added to the external solutions (0.5 or 0.05 μM).

To record Cl^- currents, voltage test pulses from −100 to +100 m*V* at 20-m*V* increments were applied every 4 s for a duration of 0.75 s. At the end of each test pulse, the membrane was hyperpolarized to −100 m*V* for 0.1 s. Between pulses, cells were clamped to a holding potential of 0 m*V*. Current−voltage relations were determined from the current at the end of the test pulse. An Ag-AgCl electrode was used to ground the bath through a 3 M KCl agar bridge. Experiments were conducted at room temperature (20–24°C).

The relative permeabilities of $Glut^-$ and Cl^- (P_{Glut}/P_{Cl}) were calculated from the current reversal potentials (V_r) corrected for liquid junction potentials using the Junction Potential Calculator (Axon Instruments). Corrected V_r values were substituted into a standard form of the Goldman-Hodgkin-Katz equation, rearranged to solve for the permeability ratio:

$$\frac{P_{Glut^-}}{P_{Cl^-}} = \frac{e^{V_r\,(zF/RT)}\,[Cl^-]_{out} - [Cl^-]_{in}}{[Glut^-]_{in} - e^{V_r\,(zF/RT)}\,[Glut^-]_{out}}$$

where *z*, *F*, *R* and *T* have their usual meanings.

Preparation of Membrane-Associated Proteins

Affinity-enriched plasma membrane proteins were isolated from the parotid gland acinar cells or from HEK293 cells by biotinylation as previously described (Gonzalez-Begne et al. 2007). Briefly, mice were anesthetized with CO_2 gas and killed by exsanguination via cardiac puncture. Glands were finely minced and digested two times (10 min each) in 0.17 mg/ml liberase RI enzyme (Roche Applied Science, Indianapolis, IN) to enrich for parotid gland acinar cells. Acinar cells or HEK293 cells 24 h posttransfection were incubated in ice-cold PBS containing 0.5 mg/ml of EZ-Link Sulfo NHS-SS-biotin on a rocking platform (Speci-Mix; Thermolyne/Fisher Scientific, Pittsburgh, PA) for 45 min at 4°C. The biotinylation reaction was quenched with ice-cold PBS containing 0.1 M glycine, followed by two washes of ice-cold PBS buffer.

The biotin-labeled parotid acinar cells were suspended in ice-cold homogenizing buffer containing 250 mM sucrose (J. T. Baker), 10 mM triethanolamine, 1 μg/ml leupeptin and 0.1 mg/ml phenylmethylsulfonyl fluoride. Cells were homogenized with a glass–Teflon tissue grinder (20 passes; Wheaton Science Products, Millville, NJ) and then centrifuged at 4,000 × *g* for 10 min at 4°C The supernatant was saved, the pellet resuspended and centrifuged as before and the collected supernatants pooled and centrifuged at 22,000 × *g* for 20 min at 4°C. The pellet was suspended in the same buffer and centrifuged at 46,000 × *g* (SS28 rotor; Beckman, Fullerton, CA) for 30 min at 4°C. The resultant crude pellet was resuspended in hypotonic buffer (containing 100 mM NH_4HCO_3 [pH 7.5], 5 mM $MgCl_2$) and then incubated with Dynabeads M-280 Streptavidin (Invitrogen) at 4°C overnight. The streptavidin beads were collected with a magnetic plate and suspended in 100 mM DTT for 2 h according to the manufacturer's instructions (DynalBiotech) and then centrifuged at 10,600 × *g* for 3 min. The supernatants were collected and used for electrophoresis and Western blot analysis.

The biotin-labeled HEK293 cells were lysed by incubation in radioimmunoprecipitation assay buffer (0.1% sodium dodecyl sulfate [SDS], 0.15 M NaCl, 1% sodium deoxycholate and 1% Triton X-100) containing 1x protease inhibitor cocktail for 30 min on ice. The lysates were sonicated using five 1-s bursts (Sonifier S-450A; Branson, Danbury, CT) and centrifuged at 14,000 × *g* for 10 min at 4°C. The clarified supernatants were incubated overnight at 4°C with immobilized neutravidin protein crosslinked to agarose beads with end-over-end mixing on a Labquake shaker (Labindustries, Berkeley, CA). The biotinylated proteins bound to the neutravidin beads were washed with buffer containing 1x protease inhibitor cocktail (Pierce). SDS-polyacrylamide gel electrophoresis (Non-Reducing

Lane Marker, 5x; Pierce) sample buffer containing 50 mM DTT was added to the beads, incubated at room temperature for 1 h with end-over-end mixing and then heated at 55°C for 20 min to release the biotinylated proteins upon cleavage of the disulfide bond in the spacer arm.

Crude plasma membranes were isolated from the heart as above except the hearts were initially perfused via the left ventricle with PBS. Minced hearts were suspended in ice-cold homogenizing buffer containing 250 mM sucrose (J. T. Baker), 10 mM triethanolamine, 1 μg/ml leupeptin and 0.1 mg/ml phenylmethylsulfonyl fluoride. Cells were homogenized with a glass–Teflon tissue grinder (20 passes, Wheaton Science Products) and centrifuged at 4,000 × *g* for 10 min at 4°C. The supernatant was saved and the pellet resuspended and centrifuged in the same volume of homogenization buffer as before. The collected supernatants were pooled and centrifuged at 22,000 × *g* for 20 min at 4°C. The pellet was suspended in the same buffer and centrifuged at 46,000 × *g* (Beckman SS28 rotor) for 30 min at 4°C to obtain a crude plasma membrane faction.

Immunoprecipitation of Best3 Proteins

Precipitation of Best3 and Best3-Δ2,3,6 proteins was performed using the Seize® X Protein A Immunoprecipitation kit according to the manufacturer's instructions (Pierce). ImmunoPure® immobilized protein A plus was incubated with 25 μg of purified rabbit polyclonal to *Best-4* (Abcam, Cambridge, MA) for 30 min at room temperature by end-over-end mixing on a Labquake shaker. Bound antibody was cross-linked by addition of No-weigh™ disuccinimidyl suberate (DSS, Pierce) in dimethyl sulfoxide (DMSO, Sigma-Aldrich) for 60 min at room temperature. The reaction was quenched with ImmunoPure® elution buffer (pH 2.8), followed by binding/washing buffer (BupH™ Modified Dulbecco's PBS, Pierce). The biotinylated-parotid membrane fraction and the heart membrane proteins were immunoprecipitated by incubation with cross-linked protein A overnight at 4°C. The beads were thoroughly washed with binding/washing buffer, the antigens were eluted with Immunopure® Elution buffer (Pierce) and then 1 M Tris (pH 9.5) was added to neutralize the precipitated protein prior to Western blot analysis.

Electrophoresis and Western Blot Analysis

The immunoprecipitated proteins (~20 μg of total protein) were reduced in 10 μl of 5x lane marker sample buffer containing 6 μl of 1 M DTT stock solution (Calbiochem/EMD Biosciences, San Diego, CA) and separated in a 7.5% SDS-PAGE Tris-glycine minigel (Bio-Rad). Reduced samples from HEK293 cells containing about 30 μg of total protein were separated in a 10% SDS-PAGE Tris-glycine minigel. Proteins were transferred onto polyvinylidene (PVDF) membranes (Invitrogen) overnight at 4°C using a transfer buffer containing 10 mM 3-[cyclohexylamino]-1-propanesulfonic acid (CAPS, pH 11) in 10% methanol. The membranes were blocked overnight at 4°C with 5% nonfat dry milk in 25 mM Tris (pH 7.5), 150 mM NaCl (TBS) and then incubated with either the polyclonal anti-Best4 (Abcam; Best4 has been renamed Best3, see "Introduction") or anti-Best3 (generously provided by Dr. Criss Hartzell) antibody at a dilution of 1:500 or 1:1,000, respectively, in 2.5% nonfat dry milk solution at 4°C overnight. The anti-Best4 antibody recognizes the C-terminal epitope of mouse Best-3 (residues 652–669), and the target sequence used to generate the anti-Best3 antibody from Dr. Hartzell overlaps with that from Abcam, recognizing the final 200 amino acids in the C-terminus of mouse Best3 (residues 470–669). After washing with TBS containing 0.1% Tween-20 (TBS-T), membranes were incubated with horseradish peroxidase–conjugated goat-anti rabbit IgG secondary antibody (Pierce) at a dilution of 1:2,500 in TBS-T/2.5% nonfat dry milk for 1 h at room temperature. Labeled proteins were visualized using enhanced chemiluminescence (ECL detection kit; GE-Amersham Biosciences, Piscataway, NJ).

Results

Best3 Splice Variants

The murine *Best3* gene (*Vmd2l3*, accession number NM_001007583) is composed of 10 exons that transcribe multiple splice variants, each of which displays tissue-specific expression (Kramer et al. 2004). To examine the expression of these multiple splice variants in exocrine glands (pancreas, lacrimal and salivary glands) and other tissues, primer set A (Table 1, Fig. 1a) was used to amplify the coding region including exons 1–7 by reverse transcription (RT) PCR. Several splice variants of Best3 were amplified in different tissues (Fig. 2). Heart and testis expressed multiple variants, confirming the results of Kramer et al. (2004). Variant 1, the largest visible band, was detected only in the heart. Expression of variants 4 and 5 was confirmed in kidney, lung, liver and testis. The lacrimal gland expressed only variant 5 (Best3-Δ2,3,6); however, parotid, submandibular and sublingual glands expressed both variants 4 and 5. Best3 expression was not detected using primer set A (Table 1) in the pancreas, spleen or lymph node.

Cloning of Best3 (Variant 1) and Best3-Δ2,3,6 (Variant 5)

To compare the functional properties of the Best3-Δ2,3,6 splice variant found in the salivary and lacrimal glands and

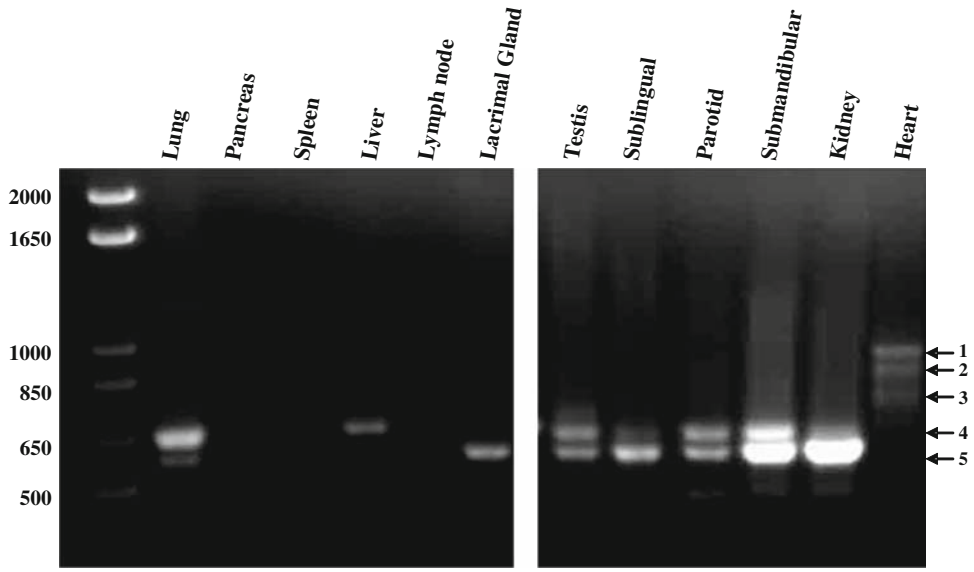

Fig. 2 Alternative splicing of Best3 transcripts. RT-PCR expression analysis of Best3 transcripts in different organ tissues was performed with primers located in exon 1 and exon 7 (Table 1, Fig. 1A). The variant numbers indicated are based on sequencing results as well as predictions from Kramer et al. (2004). Five unique splice variants were observed. Variant 5, also termed Best3-Δ2,3,6, was expressed in numerous tissues, including most exocrine glands

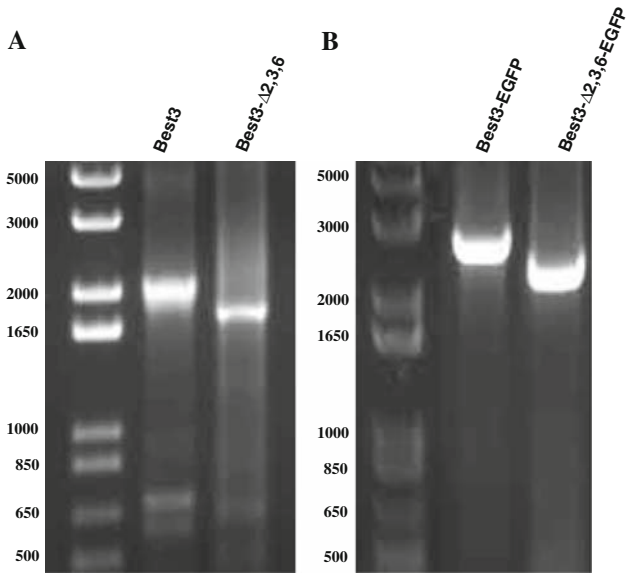

Fig. 3 Expression of Best3 and Best3-Δ2,3,6. (**A**) RT-PCR amplified Best3 (heart, *lane 1*) and Best3-Δ2,3,6 (parotid gland, *lane 2*). Primer set B was used to amplify the coding region from exon 1 to exon 10 (see Table 1 and Fig. 1b). The resulting amplified PCR products of Best3 (2,162 bp) and Best3-Δ2,3,6 (1,821 bp) were cloned into the TOPO vector and sequences. (**B**) RT-PCR-amplified Best3-EGFP fusion (*lane 1*) and Best3-Δ2,3,6-EGFP fusion (*lane 2*). Primer sets G and H (Table 1) were used. The resulting amplified PCR products of Best3-EGFP (2,765 bp) and Best3-Δ2,3,6-EGFP (2,368 bp) were cloned into the pEGFPN1 vector to express an EGFP fusion protein (see Fig. 4)

the full-length Best3, we amplified the open reading frames of the full-length Best3 from heart and Best3-Δ2,3,6 from the parotid gland using primer set B (Table 1, Fig. 1b). The sequence of the resultant PCR product from heart Best3 was identical to that in the NCBI nucleotide databank (accession NM_001007583). The first ATG start codon was located in exon 2. Full-length Best3 consisted of 2,162 bp, predicted to contain 2,007 bp of coding region that would translate a 669–amino acid protein (Fig. 3a, lane 1). In contrast, the PCR product amplified from the parotid (Best3-Δ2,3,6) was 1,821 bp, with 1,611 bp (537 amino acids) of coding sequence (Fig. 3a, lane 2). Analysis of the Best3-Δ2,3,6 sequence revealed that alternate splicing deleted exons 2, 3 and 6, generating an in-frame protein that lacks 132 of the predicted 669 amino acids. Full-length Best3 used the ATG codon located in exon 2; however, Best3-Δ2,3,6, which lacked exons 2 and 3, used an alternative ATG initiation codon located in exon 4. The deleted amino acids comprise the cytoplasmic N-terminus and the initial two predicted transmembrane domains (aa 1–106). Moreover, the loss of exon 6 in Best3-Δ2,3,6 deleted part of a predicted hydrophobic loop (aa 213–238 in full-length Best3). Because the number of transmembrane domains in this protein is uncertain, the intracellular vs. extracellular location of this latter deletion is unclear (Milenkovic et al. 2007; Qu et al. 2007; Sun et al. 2002; Tsunenari et al. 2003).

The full-length Best3 and Best3-Δ2,3,6 variants were cloned into the biscistronic pIRES-EGFP vector for functional analysis. Full-length Best3 was amplified using primer set C, while Best3-Δ2,3,6 was amplified using primer set D (Fig. 1, Table 1). Both sets of primers used the same reverse primer, which is located 3' to the stop codon in exon 10, but the forward primers for Best3 and Best-Δ2,3,6 are located in exon 2 (Fig. 1c) and exon 1 (Fig. 1d), respectively. The Best3 and Best-Δ2,3,6 cDNAs were also cloned in-frame into the pEGFPN1 vector to express Best-EGFP and Best-Δ2,3,6–EGFP fusion proteins. Figure 3b shows that the predicted 2,765 bp Best-EGFP fusion product (lane 1) and the 2,368 bp Best-Δ2,3,6–EGFP (lane 2) fusion products were generated.

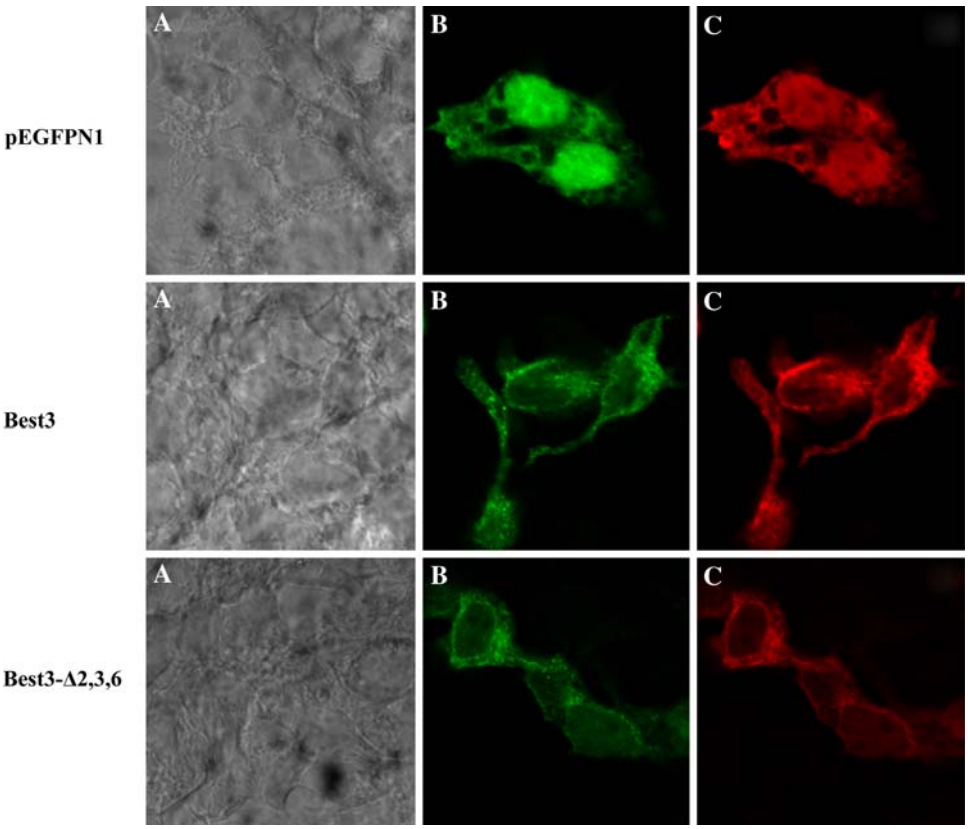

Fig. 4 Localization of Best3–EGFP, Best3-Δ2,3,6–EGFP and EGFP proteins expressed in HEK293 cells. HEK293 cells were transiently transfected with empty vector (pEGFPN1), Best3–EGFP or Best3-Δ2,3,6–EGFP. (**A**) Differential interference contrast images. (**B**) EGFP fluorescence. (**C**) Cells labeled using an anti-GFP antibody and a rhodamine-tagged secondary antibody. Fluorescence images were viewed by confocal microscopy. The thickness of the sections was estimated to be around 7 μm

Localization of Best-Δ2,3,6 and Full-Length Best3

Best3 and Best-Δ2,3,6 were expressed in HEK293 cells by transfection with either Best-EGFP or Best-Δ2,3,6–EGFP containing vectors (Table 1). Localization of Best-EGFP and Best-Δ2,3,6–EGFP was visualized either by directly monitoring EGFP fluorescence (Fig. 4b) or with an anti-GFP antibody (Fig. 4c). As expected, EGFP was diffusely distributed in both the nucleus and the cytosol (Fig. 4b, c; pEGFPN1). In contrast, the nucleus excluded the Best3 and Best-Δ2,3,6 EGFP fusion proteins, while some targeted near the plasma membrane (Fig. 4b, Best3 and Best-Δ2,3,6). Considerable Best-EGFP and Best-Δ2,3,6–EGFP accumulation was also present as punctate structures in the cytosolic compartment (Fig. 4b, Best3 and Best-Δ2,3,6). Localization of Best-EGFP and Best-Δ2,3,6–EGFP using the anti-GFP antibody gave a similar pattern (Fig. 4c, Best3 and Best-Δ2,3,6) in permeabilized cells, but non-permeabilized cells failed to stain (not shown). This latter result indicated that the C-termini of both Best3 and Best-Δ2,3,6 are within the cytoplasmic compartment and, thus, inaccessible to the antibody. These data are consistent with the predicted structural models of Best proteins (Milenkovic et al. 2007; Qu et al. 2007; Sun et al. 2002; Tsunenari et al. 2003).

Our localization studies suggested that some of the expressed Best-Δ2,3,6 and Best3 targeted near the plasma membrane. To confirm that the expressed Best-Δ2,3,6 and Best3 proteins inserted into the plasma membrane, exposed extracellular sites were biotinylated in intact HEK293 cells transfected with either the Best3 or Best-Δ2,3,6 construct and the plasma membrane was subsequently isolated by affinity chromatography for Western blot analysis using an anti-Best3 antibody. The anti-Best3 antibody labeled a unique protein with a molecular weight consistent with the predicted size of Best3 (76.4 kDa) in the blot generated from HEK293 cells transfected with the Best3 construct (Fig. 5a, lane 1), while transfection with the Best-Δ2,3,6 construct yielded the expected 60.5-kDa molecular weight protein (Fig. 5a, lane 2). Several other protein bands were also labeled by the anti-Best3 antibody. Figure 5a shows that these bands were nonspecific because they were also present in cells transfected with empty vector/lipofectamine or treated with lipofectamine only (lanes 3 and 4, respectively), but no staining was detected at the predicted molecular weights of Best3 or Best-Δ2,3,6. Plasma membrane fractions from cells expressing Best-EGFP or Best-Δ2,3,6–EGFP contained the expected molecular weight EGFP fusion proteins in transfected HEK293 cells as well (not shown).

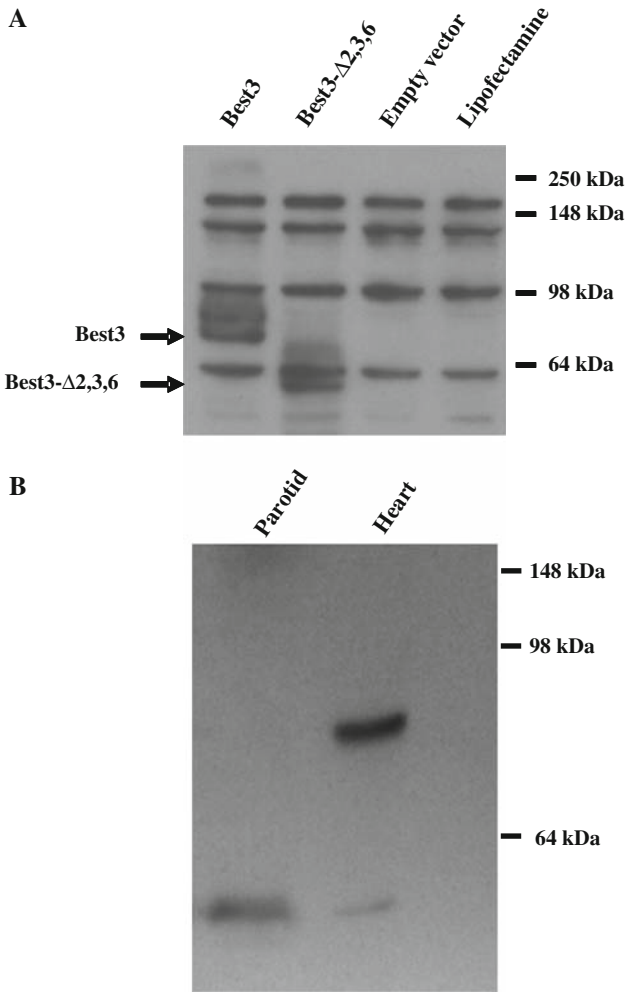

Fig. 5 Western blot analysis of Best3 and Best3-Δ2,3,6. (**A**) Western blot analysis of the biotinylated plasma membrane proteins isolated from HEK293 cells transiently expressing Best3 (*lane 1*) and Best3-Δ2,3,6 (*lane 2*) using an anti-Best3 antibody kindly provided by Dr. Criss Hartzell. The expected molecular weights of Best3 and Best3-Δ2,3,6 are 76.4 and 60.5 kDa, respectively. *Lanes 3* and *4* show biotinylated proteins isolated from cells transfected with empty vector and nontransfected, lipofectamine-treated cells, respectively. (**B**) Western blot analysis using an anti-Best3 antibody (Abcam) detected proteins of the expected molecular weights of Best3 and Best3-Δ2,3,6 in the biotinylated plasma membrane proteins isolated from mouse parotid salivary glands and membrane proteins from heart (*lanes 1* and *2*, respectively). Similar results were obtained using an antibody provided by Dr. Criss Hartzell. Both antibodies labeled proteins of the expected molecular weights of Best3 and Best3-Δ2,3,6 (76.4 and 60.5 kDa, respectively). Note that the heart contains a faint band with a molecular weight consistent with Best3-Δ2,3,6 expression

Proteins of the expected molecular weight for Best3 and the Best-Δ2,3,6 splice variant were also expressed in the heart and parotid glands, respectively (Fig. 5b). The anti-Best3 antibody detected an approximately 60-kDa band in the biotinylated plasma membrane protein isolated from mouse parotid glands (Fig. 5b, lane 1). This antibody also detected an approximately 76-kDa protein in the membranes isolated from mouse heart (Fig. 5b, lane 2). Note that there is also a faint protein band in the heart at the predicted size of the Best-Δ2,3,6 splice variant. Together, our results are consistent with Best3 and Best-Δ2,3,6 expression in these native tissues.

Functional Characterization of Best3 and Best3-Δ2,3,6

The whole-cell patch-clamp technique was used to determine if the full-length Best3 transcript isolated from the heart encodes a functional Ca^{2+}-dependent Cl channel. Figure 6 demonstrates that HEK293 cells transfected with Best3 displayed Cl^- currents in the presence of 1 μM Ca^{2+} (14 ± 4 pA/pF at +100 m*V*, $n = 12$), while both nontransfected cells and cells transfected with Best3 with zero intracellular Ca^{2+} showed essentially no current (2.1 ± 0.2 pA/pF, $n = 4$ and 3 ± 1 pA/pF, $n = 4$, respectively; not shown). The Best3 current had little voltage or time dependence as previously shown using essentially identical experimental conditions (Qu et al. 2006; Tsunenari et al. 2003, 2006). The current was modestly sensitive to DIDS, a general Cl channel inhibitor (Fig. 6). Superfusion of the cells with 0.05 or 0.5 mM DIDS inhibited the current at +100 m*V* by $12 \pm 3\%$ and $64 \pm 9\%$ ($n = 5$ and 7, respectively), with less inhibition at −100 m*V* ($2 \pm 3\%$ and $46 \pm 8\%$ with 0.05 or 0.5 mM DIDS, respectively). DIDS blockade of native parotid acinar Ca^{2+}-dependent Cl^- currents as well as exogenously expressed hBest1 currents has been previously shown to be voltage-dependent, while inhibition of mBest2 currents was voltage-independent (Arreola, Melvin and Begenisich 1995; Qu et al. 2004; Sun et al. 2002). The reversal potential (-3 ± 2 m*V*, $n = 12$) was consistent for an anion-selective channel recorded in nearly symmetrical

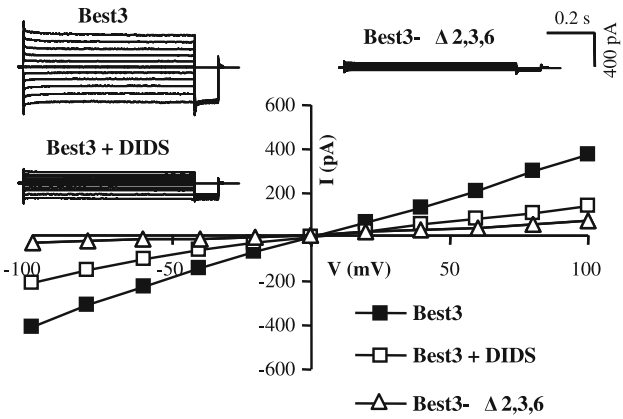

Fig. 6 DIDS-sensitive, Ca^{2+}-activated Cl^- currents of heterologously expressed Best3. Typical current traces (*upper panels*) and *I-V* plot (*lower panel*) recorded in HEK293 cells transiently transfected with Best3-Δ2,3,6 (Δ) or Best3 either in the absence (■) or in the presence (□ = 500 μM) of DIDS. Currents were recorded in symmetric Cl^- solutions

[Cl^-] conditions. However, a linear leak current on top of the linear Ca^{2+}-dependent Cl^- currents, as those produced by expression of Best3, would also give a reversal potential near 0 m*V*. Therefore, to confirm that Best3 expression produced chloride-selective currents, we substituted NaCl for Na-glutamate in the bath solution. Taking into consideration the small permeability of Ca^{2+}-dependent Cl channels to glutamate, chloride substitution resulted in the expected positive shift of the reversal potential (+48 ± 3 m*V*, $n = 4$).

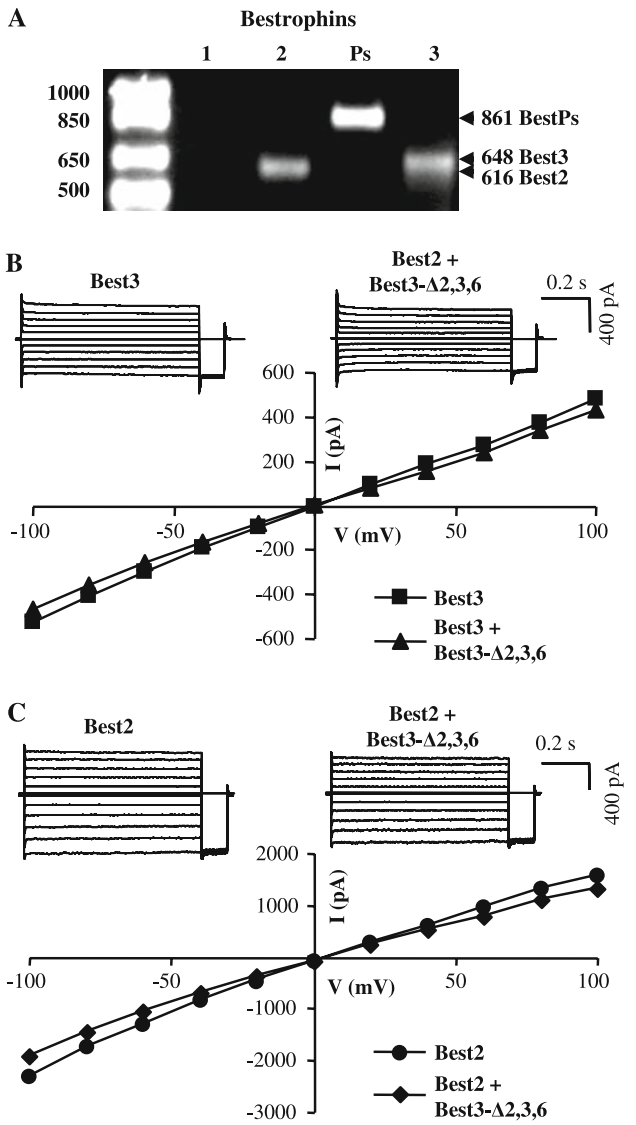

Fig. 7 Best2 and Best3 Ca^{2+}-activated Cl^- currents coexpressed with Best3-Δ2,3,6. (**A**) Results of PCR amplification of Best1, Best2, BestPs and Best3 in isolated mouse parotid acinar cells. Best1 was not detected, while the Best2, BestPs and Best3 primers generated the expected size amplification products. Products were sequence-verified. (**B**, **C**) Typical current traces (*upper panels*) and *I–V* plots (*lower panels*) recorded in HEK293 cells stably expressing either Best3 alone or Best3 transiently cotransfected with Best3-Δ2,3,6 (**B**) or Best2 alone or Best2 cotransfected with Best3-Δ2,3,6 (**C**). Currents were recorded in symmetric Cl^- solutions

Using the determined reversal potentials, we evaluated the P_{Glu}/P_{Cl} permeability ratio (see "Materials and Methods"). The calculated P_{Glu}/P_{Cl} value of 0.10 ± 0.02 is close to the previously reported permeability ratio for the Ca^{2+}-dependent Cl currents in rat parotid acinar cells ($P_{Glu}/P_{Cl} = 0.05$ and 0.09 [Perez-Cornejo et al. 2004, and Ishikawa 1996], respectively).

In contrast to cells expressing Best3, cells transfected with Best-Δ2,3,6 lacked Ca^{2+}-dependent Cl^- currents (Fig. 6). The mean current density measured at +100 m*V* was 2.0 ± 0.4 pA/pF ($n = 7$), comparable to the mean current density measured in nontransfected cells and cells transfected with full-length Best3 with zero intracellular Ca^{2+} (see above). This amount of "leak" current is the expected minimal background current with a patch resistance of several gigaohms and a cell capacitance of 18 ± 3 pF ($n = 7$).

It has been proposed that the minimal functional unit of Bestrophins is dimeric (Stanton et al. 2006; Sun et al. 2002) and that mutations in Best channels can dominantly inhibit wild-type channels (Sun et al. 2002). In Fig. 7a, we determined by PCR that Best2 and Best3, but not Best1, transcripts are expressed in acinar cells isolated from mouse parotid glands. Thus, we coexpressed Best2 or Best3 with Best-Δ2,3,6 to determine if this spliced protein variant modulates the activity of these full-length channels. However, cotransfection of Best-Δ2,3,6 had no significant effect on the amplitude of the Ca^{2+}-dependent Cl^- currents associated with full-length Best3 expression (Fig. 7b: 12 ± 4 pA/pF [$n = 6$] vs. 14 ± 4pA/pF [$n = 5$] for Best3 alone vs. Best3/Best-Δ2,3,6, respectively) or Best2 expression (Fig. 7c: 43 ± 7 pA/pF [$n = 6$] vs. 40 ± 5 pA/pF [$n = 6$] Best2 alone vs. Best2/Best-Δ2,3,6, respectively). The time and voltage dependence of the currents observed in cells transfected with Best2 or Best3 alone and Best2 or Best3 cotransfected with Best-Δ2,3,6 were also similar (Fig. 7). Moreover, cotransfection with Best-Δ2,3,6 did not significantly affect the P_{Glu}/P_{Cl} permeability ratio of Best3 (0.11 ± 0.02, $n = 4$) or Best2 (0.07 ± 0.03, $n = 4$ for cotransfected vs. 0.04 ± 0.02, $n = 3$ for mBest2 alone). Overall, our functional studies demonstrate the importance of the N-terminal region of Best3. Importantly, loss of this region led to a membrane-associated, nonconducting protein (Best3-Δ2,3,6) which did not appear to modulate the functional properties of the full-length versions of the Best2 and Best3 channels.

Discussion

The completion of several DNA sequencing projects demonstrated that mammalian genomes encode approximately 20,000 genes, considerably fewer than originally

predicted. To increase the functional diversity of mammalian genomes, many genes transcribe multiple mRNAs, hundreds of variants in extreme cases, through alternate splicing and/or multiple promoter strategies. Kramer et al. (2004) performed a detailed RT-PCR analysis of the transcriptome of the *Vmd2* (*Best*) gene family in a panel of mouse tissues. Tissue-specific expression of multiple splice variants was exclusively observed for *Vmd2l3* (also known as *Best3*), suggesting that these different *Best3* gene products may have been adapted to perform unique functions. RT-PCR amplification of Best3 transcripts in brain, retina, heart, lung, kidney, skeletal muscle and testis yielded six different alternately spliced variants. The full-length variant 1 was exclusively observed in heart tissue. Loss of exon 6 in variant 2 led to an in-frame deletion of 26 amino acids. In contrast, removal of exon 3 in variant 3 resulted in a frame shift and a premature stop codon in exon 5. Splice variants 4 and 5 are widely expressed in tissues such as the brain, retina, heart, lung, kidney, skeletal muscle and testis. Both variants 4 and 5 use an alternate in-frame start codon located in exon 4 and are predicted to generate proteins with an N-terminal truncation of 106 amino acids. In addition to missing exons 2 and 3, variant 5 lacks exon 6. The brain-specific variant 6 lacks exons 2, 3 and part of 4 and is predicted to encode a protein with an N-terminal 129−amino acid truncation.

Neither the functional relevance of these numerous splice variants nor their expression in exocrine glands has been explored in detail. Northern blot analysis detected Best3 transcripts in the mouse parotid salivary gland and heart, consistent with the expression of alternately spliced and full-length variants (not shown). PCR analysis demonstrated that the heart expressed several splice variants including the full-length transcript. In contrast, we found that exocrine glands like the lacrimal, parotid, submandibular and sublingual, but not the pancreas, expressed splice variant 5 of Best3 (Best3-Δ2,3,6). It is interesting to note that unlike these other exocrine glands, the acinar cells of the pancreas produce little fluid, possibly suggesting that Best3-Δ2,3,6 is involved in fluid secretion.

Splice variant Best3-Δ2,3,6 is predicted to initiate protein translation using an ATG located in exon 4. Best3-Δ2,3,6 contains several predicted transmembrane-spanning domains but did not produce Ca^{2+}-activated chloride currents when expressed in HEK293 cells, unlike the full-length Best3 cloned from the heart. Because Best3-Δ2,3,6 did not produce Ca^{2+}-activated Cl^- currents, it was important to determine if Best3-Δ2,3,6 targets to the plasma membrane. Western blot analysis of plasma membrane protein from native parotid tissue as well as EGFP fluorescence, immunohistochemistry and biotinylation experiments in HEK293 cells suggested that Best3-Δ2,3,6 is expressed in the plasma membrane, although much of the protein remains in intracellular compartments. This latter result was not unanticipated as both hBest1 and mBest2 expression leads to cell surface expression but with considerable intracellular localization (Qu et al. 2004; Tsunenari et al. 2003).

It has been previously shown that deletion of a major part of the C-terminus of mouse Best3 produces large Cl^- currents (Qu et al. 2006, 2007). These results suggested that the C-terminal domain acts as a negative modulator of Cl channel function. Indeed, it was found that mutations in an autoinhibitory sequence (^{356}IPSFLGS^{362}) of this channel upregulate the current without calcium. On the other hand, it has been shown that transmembrane domain 2 of mouse Best2 is important in the formation of the Bestrophin pore. Mutations in several amino acids located in this transmembrane domain resulted in altered anion permeation and conduction (Qu and Hartzell 2004; Sun et al. 2002; Tsunenari et al. 2003). This region of Best2 is highly homologous with transmembrane domain 2 of Best3 (>75% identical). Thus, it is not entirely surprising that truncation of the N-terminus, including the predicted transmembrane-spanning domain 2 of Best3-Δ2,3,6, resulted in a nonfunctional channel. However, it is important to note that Bestrophin proteins form complexes (Stanton et al. 2006; Sun et al. 2002) and that mutations in Best channels can dominantly inhibit wild-type channels (Sun et al. 2002). It has been previously shown that transcripts for BEST2 are expressed in both human and mouse parotid salivary glands (Nakamoto et al. 2007). Here, we show that isolated mouse parotid acinar cells coexpress Best2 and Best3 (Fig. 7a) and that heart tissue expresses a protein consistent with Best3-Δ2,3,6 (Fig. 5b), raising the possibility that Best3-Δ2,3,6 may regulate Best2 and/or Best3 activity in these organs. Even though we found that Best3-Δ2,3,6 targeted to the plasma membrane, we did not detect modulation of Best2 or Best3 channel function when coexpressed with Best3-Δ2,3,6. These results suggested that the alternatively spliced Best3-Δ2,3,6 variant does not regulate the functional properties of the full-length Best2 and Best3 channels.

Acknowledgements We thank Laurie Koek, Mark Wagner and Jennifer Scantlin for technical assistance. We are also grateful to Dr. Ted Begenisich for discussions and critical reading of the manuscript. This work was supported in part by National Institutes of Health grants DE09692 and DE08921 (to J. E. M.).

References

Arreola J, Melvin JE, Begenisich T (1995) Inhibition of Ca^{2+}-dependent Cl^- channels from secretory epithelial cells by low internal pH. J Membr Biol 147:95–104

Arreola J, Melvin JE, Begenisich T (1996a) Activation of calcium-dependent chloride channels in rat parotid acinar cells. J Gen Physiol 108:35–47

Arreola J, Melvin JE, Begenisich T (1996b) Three distinct chloride channels control anion movements in rat parotid acinar cells. J Physiol 490:351–62

Arreola J, Melvin JE, Begenisich T (1998) Differences in regulation of Ca^{2+}-activated Cl^- channels in colonic and parotid secretory cells. Am J Physiol 274:C161–C166

Barro Soria R, Spitzner M, Schreiber R, Kunzelmann K (2006) Bestrophin 1 enables Ca^{2+} activated Cl^- conductance in epithelia. J Biol Chem. doi: 10.1074/jbc.M605716200

Chien LT, Zhang ZR, Hartzell HC (2006) Single Cl^- channels activated by Ca^{2+} in *Drosophila* S2 cells are mediated by bestrophins. J Gen Physiol 128:247–259

Duta V, Szkotak AJ, Nahirney D, Duszyk M (2004) The role of bestrophin in airway epithelial ion transport. FEBS Lett 577:551–554

Eggermont J (2004) Calcium-activated chloride channels: (un)known, (un)loved? Proc Am Thorac Soc 1:22–27

Evans MG, Marty A (1986) Calcium-dependent chloride currents in isolated cells from rat lacrimal glands. J Physiol 378:437–460

Fuller CM, Benos DJ (2000) Ca^{2+}-activated Cl^- channels: a newly emerging anion transport family. News Physiol Sci 15:165–171

Gonzalez-Begne M, Nakamoto T, Nguyen HV, Stewart AK, Alper SL, Melvin JE (2007) Enhanced formation of a HCO_3^- transport metabolon in exocrine cells of $Nhe1^{-/-}$ mice. J Biol Chem 282:35125–35132

Hartzell C, Putzier I, Arreola J (2005) Calcium-activated chloride channels. Annu Rev Physiol 67:719–758

Ishibashi K, Yamazaki J, Okamura K, Teng Y, Kitamura K, Abe K (2006) Roles of CLCA and CFTR in electrolyte re-absorption from rat saliva. J Dent Res 85:1101–1105

Ishikawa T (1996) A bicarbonate- and weak acid-permeable chloride conductance controlled by cytosolic Ca^{2+} and ATP in rat submandibular acinar cells. J Membr Biol 153:147–159

Kidd JF, Thorn P (2000) Intracellular Ca^{2+} and Cl^- channel activation in secretory cells. Annu Rev Physiol 62:493–513

Kotera T, Brown PD (1993) Calcium-dependent chloride current activated by hyposmotic stress in rat lacrimal acinar cells. J Membr Biol 134:67–74

Kramer F, Stohr H, Weber BH (2004) Cloning and characterization of the murine Vmd2 RFP-TM gene family. Cytogenet Genome Res 105:107–114

Kunzelmann K, Milenkovic VM, Spitzner M, Soria RB, Schreiber R (2007) Calcium-dependent chloride conductance in epithelia: is there a contribution by Bestrophin? Pfluegers Arch 454:879–889

Loewen ME, Forsyth GW (2005) Structure and function of CLCA proteins. Physiol Rev 85:1061–1092

Martin DK (1993) Small conductance chloride channels in acinar cells from the rat mandibular salivary gland are directly controlled by a G-protein. Biochem Biophys Res Commun 192:1266–1273

Marty A, Tan YP, Trautmann A (1984) Three types of calcium-dependent channel in rat lacrimal glands. J Physiol 357:293–325

Melvin JE, Yule D, Shuttleworth T, Begenisich T (2005) Regulation of fluid and electrolyte secretion in salivary gland acinar cells. Annu Rev Physiol 67:445–469

Milenkovic VM, Rivera A, Horling F, Weber BH (2007) Insertion and topology of normal and mutant bestrophin-1 in the endoplasmic reticulum membrane. J Biol Chem 282:1313–1321

Mircheff AK (1989) Lacrimal fluid and electrolyte secretion: a review. Curr Eye Res 8:607–617

Nakamoto T, Srivastava A, Romanenko VG, Ovitt CE, Perez-Cornejo P, Arreola J, Begenisich T, Melvin JE (2007) Functional and molecular characterization of the fluid secretion mechanism in human parotid acinar cells. Am J Physiol 292:R2380–R2390

Perez-Cornejo P, De Santiago JA, Arreola J (2004) Permeant anions control gating of calcium-dependent chloride channels. J Membr Biol 198:125–133

Qu Z, Wei RW, Mann W, Hartzell HC (2003) Two bestrophins cloned from Xenopus laevis oocytes express Ca^{2+}-activated Cl^- currents. J Biol Chem 278:49563–49572

Qu Z, Fischmeister R, Hartzell C (2004) Mouse bestrophin-2 is a bona fide Cl^- channel: identification of a residue important in anion binding and conduction. J Gen Physiol 123:327–340

Qu Z, Hartzell C (2004) Determinants of anion permeation in the second transmembrane domain of the mouse bestrophin-2 chloride channel. J Gen Physiol 124:371–382

Qu Z, Cui Y, Hartzell C (2006) A short motif in the C-terminus of mouse bestrophin 3 [corrected] inhibits its activation as a Cl channel. FEBS Lett 580:2141–2146

Qu ZQ, Yu K, Cui YY, Ying C, Hartzell C (2007) Activation of bestrophin Cl^- channels is regulated by C-terminal domains. J Biol Chem 282:17460–17467

Stanton JB, Goldberg AF, Hoppe G, Marmorstein LY, Marmorstein AD (2006) Hydrodynamic properties of porcine bestrophin-1 in Triton X-100. Biochim Biophys Acta 1758:241–247

Stohr H, Marquardt A, Nanda I, Schmid M, Weber BH (2002) Three novel human VMD2-like genes are members of the evolutionary highly conserved RFP-TM family. Eur J Hum Genet 10:281–284

Sun H, Tsunenari T, Yau KW, Nathans J (2002) The vitelliform macular dystrophy protein defines a new family of chloride channels. Proc Natl Acad Sci USA 99:4008–4013

Sundermeier T, Matthews G, Brink PR, Walcott B (2002) Calcium dependence of exocytosis in lacrimal gland acinar cells. Am J Physiol 282:C360–C365

Suzuki M (2006) The *Drosophila* tweety family: molecular candidates for large-conductance Ca^{2+}-activated Cl^- channels. Exp Physiol 91:141–147

Tsunenari T, Sun H, Williams J, Cahill H, Smallwood P, Yau KW, Nathans J (2003) Structure–function analysis of the bestrophin family of anion channels. J Biol Chem 278:41114–41125

Tsunenari T, Nathans J, Yau KW (2006) Ca^{2+}-activated Cl^- current from human bestrophin-4 in excised membrane patches. J Gen Physiol 127:749–754

Zeng W, Lee MG, Yan M, Diaz J, Benjamin I, Marino CR, Kopito R, Freedman S, Cotton C, Muallem S, Thomas P (1997) Immuno and functional characterization of CFTR in submandibular and pancreatic acinar and duct cells. Am J Physiol 273:C442–C455